

RESEARCH

Open Access



A novel ferroptosis-related 12-gene signature predicts clinical prognosis and reveals immune relevancy in clear cell renal cell carcinoma

Yingkai Hong¹, Mingen Lin¹, Dehua Ou^{1,2}, Zhuangkai Huang^{1,2} and Peilin Shen^{1*}

Abstract

Background: Clear cell renal cell carcinoma (ccRCC) is still highly aggressive and lethal even with various therapeutic approaches. As the kidney is an iron metabolism-related organ, exploring and assessing the clinical value of ferroptosis, an iron-dependent regulated cell death, is practical and important.

Methods: Prognostic ferroptosis-related differentially expressed genes (DEGs) were identified from the KIRC cohort in the cancer genome atlas (TCGA) database, from which a prognostic signature was established using Lasso-penalized Cox regression analysis. Each patient in the KIRC cohort and the E-MTAB-1980 cohort (from the ArrayExpress database) was assigned a calculated signature-correlated risk score and categorized to be either in the high- or low-risk group divided by the median risk score in the KIRC cohort. Then, the independent prognostic value of the signature was further assessed by Kaplan-Meier (K-M) survival, time-dependent receiver operating characteristic (ROC) and Cox regression analyses based on overall survival (OS) in both cohorts. Finally, risk-related DEGs were identified in both cohorts and subjected to enrichment analyses for Gene Ontology (GO), Kyoto Encyclopedia of Genes and Genomes (KEGG) and immune infiltration.

Results: Among 60 ferroptosis-related genes, 32 prognostic DEGs were identified, from which we constructed a prognostic 12-gene signature with *CARS1*, *HMGCR*, *CHAC1*, *GOT1*, *CD44*, *STEAP3*, *AKR1C1*, *CBS*, *DPP4*, *FANCD2*, *SLC1A5* and *NCOA4*. Patients in both cohorts were divided into high- and low-risk groups, which were visually distributed in two sets and had positive-risk-related mortality. The K-M survival and the ROC curves validated that the signature has prognostic value with $P < 0.05$ and area under the curve > 0.7 in both cohorts, respectively. Multivariate Cox regression further confirmed the risk score as an independent prognostic predictor for OS. Commonly enriched terms in GO and KEGG not only showed a high iron correlation but also, interestingly, immune relevance of 3 immune cells (macrophages, mast cells and regulatory T cells) and 1 immune-related function (antigen processing cell co-stimulation).

Conclusion: We established a novel 12 ferroptosis-related-gene signature that was proven to be an independent prognostic predictor for OS and inferred to be related to tumour immunity in ccRCC; however, the underlying mechanism is still poorly characterized and needs further exploration.

* Correspondence: plshen@stu.edu.cn

¹Department of Urology, The First Affiliated Hospital of Shantou University Medical College, Shantou, People's Republic of China 515041
Full list of author information is available at the end of the article



© The Author(s). 2021 **Open Access** This article is licensed under a Creative Commons Attribution 4.0 International License, which permits use, sharing, adaptation, distribution and reproduction in any medium or format, as long as you give appropriate credit to the original author(s) and the source, provide a link to the Creative Commons licence, and indicate if changes were made. The images or other third party material in this article are included in the article's Creative Commons licence, unless indicated otherwise in a credit line to the material. If material is not included in the article's Creative Commons licence and your intended use is not permitted by statutory regulation or exceeds the permitted use, you will need to obtain permission directly from the copyright holder. To view a copy of this licence, visit <http://creativecommons.org/licenses/by/4.0/>. The Creative Commons Public Domain Dedication waiver (<http://creativecommons.org/publicdomain/zero/1.0/>) applies to the data made available in this article, unless otherwise stated in a credit line to the data.

Background

As the latest research suggests, renal cell carcinoma (RCC) is the second most commonly diagnosed urological cancer after bladder cancer, in which approximately 80% are clear cell RCCs (ccRCCs) [1, 2]. Even with various therapeutic approaches, such as surgery, chemotherapy, radiotherapy, targeted therapy and the newly proposed immunotherapy, ccRCC is still one of the most difficult clinical problems in urology. Delays in diagnosis and a high metastatic rate are the main causes. The incidence of advanced ccRCC is approximately 33% at patients' first hospital visits, and 40% develop distant metastases and suffer from poor survival outcomes (the 5-year survival rate is less than 11.2%) [3]. For localized RCC, radical nephrectomy is still the major treatment modality. Concerning metastatic tumours, conventional therapeutic methods such as multitarget tyrosine kinase inhibitors (TKIs) and mammalian target of rapamycin (mTOR) inhibitors are extensively adopted; however, the therapeutic benefits are modest [4].

Iron is an essential element in the basic biological processes of the human body, and metabolic disorders are involved in the occurrence and progression of many tumours [5, 6]. Recently, iron-dependent regulated cell death (RCD), namely, ferroptosis, has drawn increasing attention in the cellular-molecular field of tumours. Less than a decade ago, ferroptosis was introduced as a nonapoptotic RCD distinguished from necroptosis [7], pyroptosis [8], and alkaliptosis [9, 10]. In 2012, Dixon et al. [11] first demonstrated that in contrast to apoptotic inhibitors, the growth inhibitory effect of erastin on RAS-mutant cancer cells can be completely antagonized by iron chelators and lipophilic antioxidants relying on a new form of RCD named ferroptosis. Morphologically, unlike typical apoptotic features such as membrane blebbing and shrinkage, classical necrosis-like features such as cell swelling and plasma membrane rupture can be observed during ferroptosis [12]. Biochemically, ferroptosis is driven by reactive oxygen species (ROS), which are highly associated with iron accumulation and lipid peroxidation [13]. Due to their high metabolic characteristics, most tumours are in a state of high oxidative stress and are required to increase their ROS scavenging ability to prevent oxidative damage, which may make them sensitive to ferroptosis [14]. Many cancers have been proven to be ferroptosis-related, such as hepatocellular carcinoma [15], gastric cancer [16, 17], ovarian cancer [18, 19], and breast cancer [20, 21]. Therefore, inducing ferroptosis to promote cell death or inhibit cell growth for cancer could be a new therapeutic strategy [22].

The kidney is an iron metabolism-related organ with biofunctions, such as balancing iron homeostasis by filtering and reabsorbing iron and promoting haemoglobin synthesis by forming erythropoietin [23]. Several studies

have demonstrated that ccRCC is highly associated with iron metabolism [24, 25]. However, the role of ferroptosis in ccRCC remains poorly understood. Thus, exploring the potential correlation between ccRCC and ferroptosis is practical and important.

To explore and assess the clinical value of ferroptosis in ccRCC, we performed this bioinformatics analysis by establishing an independent prognostic ferroptosis-related gene signature using the cancer genome atlas (TCGA) database and validated it in the ArrayExpress database. Then, common functional annotations in both cohorts were screened out with Gene Ontology (GO), Kyoto Encyclopedia of Genes and Genomes (KEGG) and immune infiltration enrichment analyses to explore the underlying mechanisms.

Methods

The flow chart of the bioinformatics analysis is presented in Fig. 1. All statistical analyses were completed in R language software (Version 4.0.3) [26], and $P < 0.05$ was considered statistically significant without a specified setting.

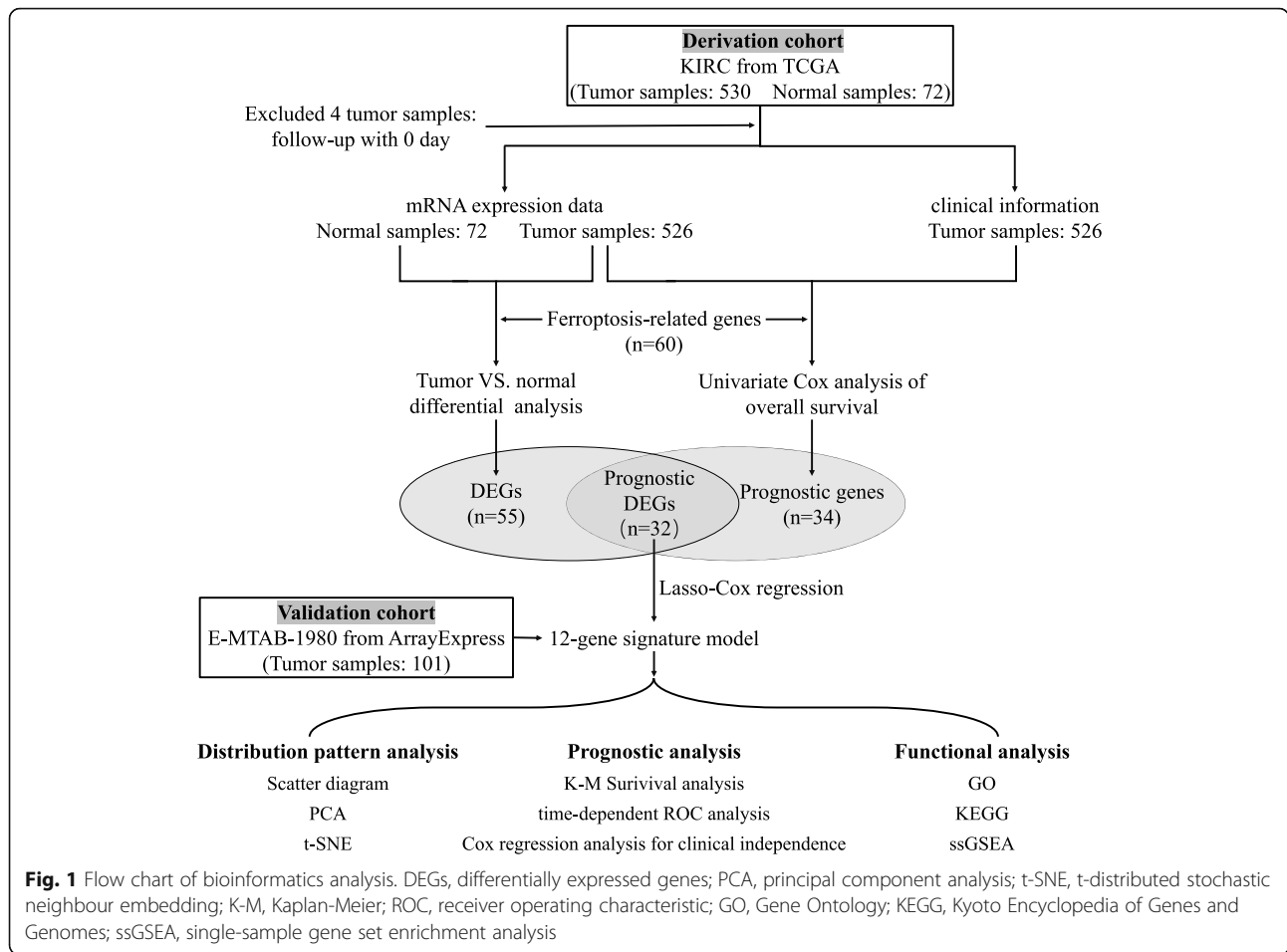
Acquisition of ferroptosis-related genes and ccRCC cohorts

A comprehensive literature survey about ferroptosis was performed, and high-quality articles were retrieved, in which 60 ferroptosis-related genes were identified and are presented in [Supplementary Table S1](#) [27–30].

The derivation set and validation set of ccRCC were retrieved from the KIRC cohort (including 526 ccRCC tissue samples and 72 normal kidney tissue samples) in the TCGA database (<https://portal.gdc.cancer.gov/repository>) and accession E-MTAB-1980 (including 101 ccRCC tissue samples) in the ArrayExpress database (www.ebi.ac.uk/arrayexpress), respectively. Both raw count values of gene expression and clinical information were downloaded from the corresponding databases. The gene expression profiles of the KIRC and E-MTAB-1980 cohorts were normalized with the "edgeR" package [31] in R language software. Patients with 0 follow-up days were removed from further analysis. Since all retrieved data were from public databases, no ethical review or approval from an Ethics Committee was required. We identified differentially expressed ferroptosis-related genes with prognostic value between ccRCC tissues and normal kidney tissues.

Identifying differentially expressed ferroptosis-related genes with prognostic value between ccRCC tissues and normal kidney tissues

The gene expression profiles of the KIRC cohort were subjected to differential expression analysis using the "edgeR" R package. Differentially expressed genes (DEGs)



between ccRCC tissues and normal kidney tissues were screened out with a false discovery rate (FDR) < 0.05 and |fold change (FC)| > 1. DEGs related to ferroptosis were selected and demonstrated with a heat map generated by the “pheatmap” R package [32]. Then, univariate Cox analysis of overall survival (OS) for 60 ferroptosis-related genes was performed to identify the genes with prognostic value. A Cox *P*-value < 0.05 indicated a significant relationship to OS. Ferroptosis-related DEGs with prognostic values were selected using intersection analysis of DEGs and prognostically valuable genes with the “Venn” R package [33] and then visualized with a protein-protein interaction (PPI) network generated by the STRING database (version 11.0) [34] and a correlation network generated by the “igraph” [35] and the “reshape2” [36] R packages.

Construction and validation of a prognostic ferroptosis-related gene signature

To minimize the risk of overfitting, we used Lasso-penalized Cox regression analysis to rule out genes with an overfitting tendency and construct a prognostic signature with the “glmnet” R package [37–39]. The risk scores in the derivation set and the validation set were

calculated according to a linear combination of the normalized expression value of each prognostic ferroptosis-related DEG and its corresponding multivariate Cox regression coefficient (β). The risk score calculation formula was as follows: Risk score = $\beta \times$ expression value of CARS1 + $\beta \times$ expression value of HMGCR + $\beta \times$ expression value of CHAC1 + $\beta \times$ expression value of GOT1 + $\beta \times$ expression value of CD44 + $\beta \times$ expression value of STEAP3 + $\beta \times$ expression value of AKR1C1 + $\beta \times$ expression value of CBS + $\beta \times$ expression value of DPP4 + $\beta \times$ expression value of FANCD2 + $\beta \times$ expression value of SLC1A5 + $\beta \times$ expression value of NCOA4. In both sets, each patient was given a risk score from the calculation of the formula and then assigned to either high- or low-risk group divided by the median risk score of the derivation set. The distribution patterns were described for the risk scores and the corresponding survival times of all patients with scatter diagrams by the “pheatmap” R package, the gene expression of established signature with principal component analysis (PCA) by the “stats” R package [26], and the patients in different risk groups with t-distributed stochastic neighbour embedding (t-SNE) by the “Rtsne” R package [40]. Kaplan-Meier (K-M) survival analysis and

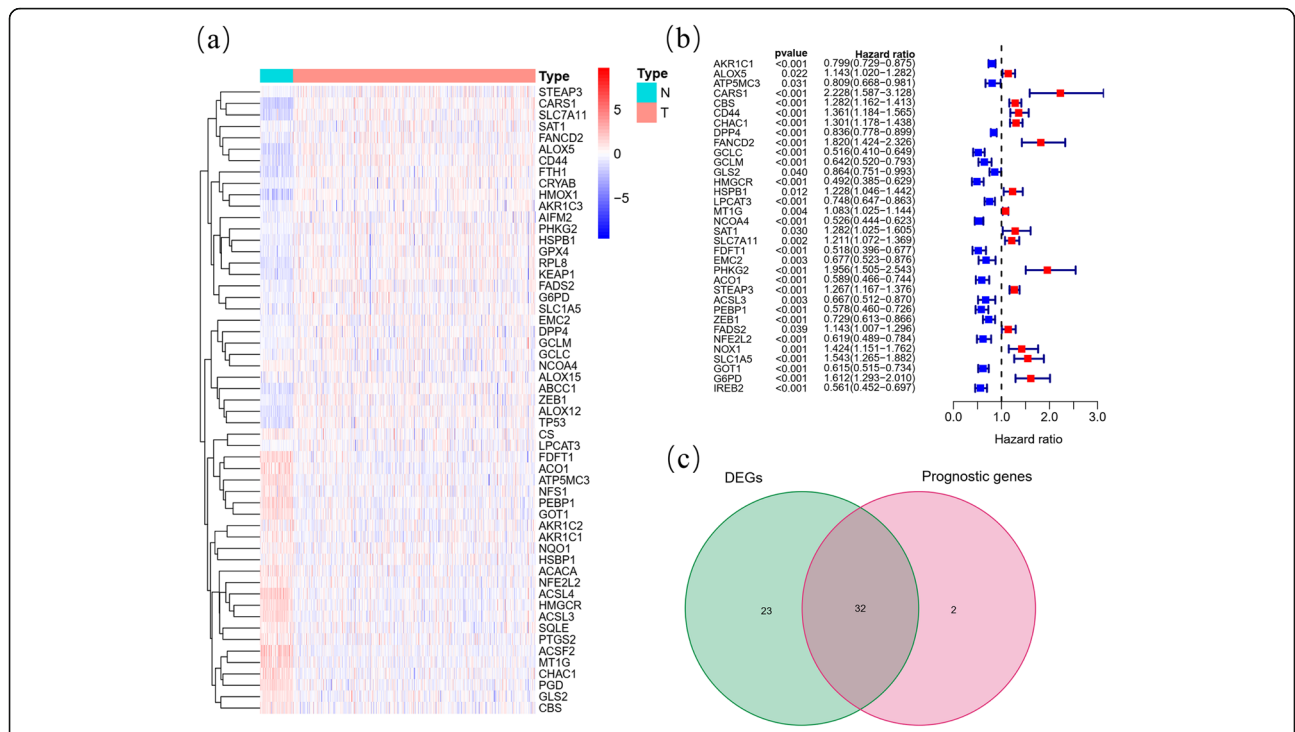


Fig. 2 Identification of the prognostic ferroptosis-related DEGs in the KIRC cohort. **(A)** Heatmap showing the ferroptosis-related DEGs identified with differential expression analysis. **(B)** Forest plots showing the significantly prognostic ferroptosis-related genes identified with univariate Cox regression analysis based on OS. **(C)** Venn diagram showing the overlapping genes between ferroptosis-related DEGs and OS-correlated genes

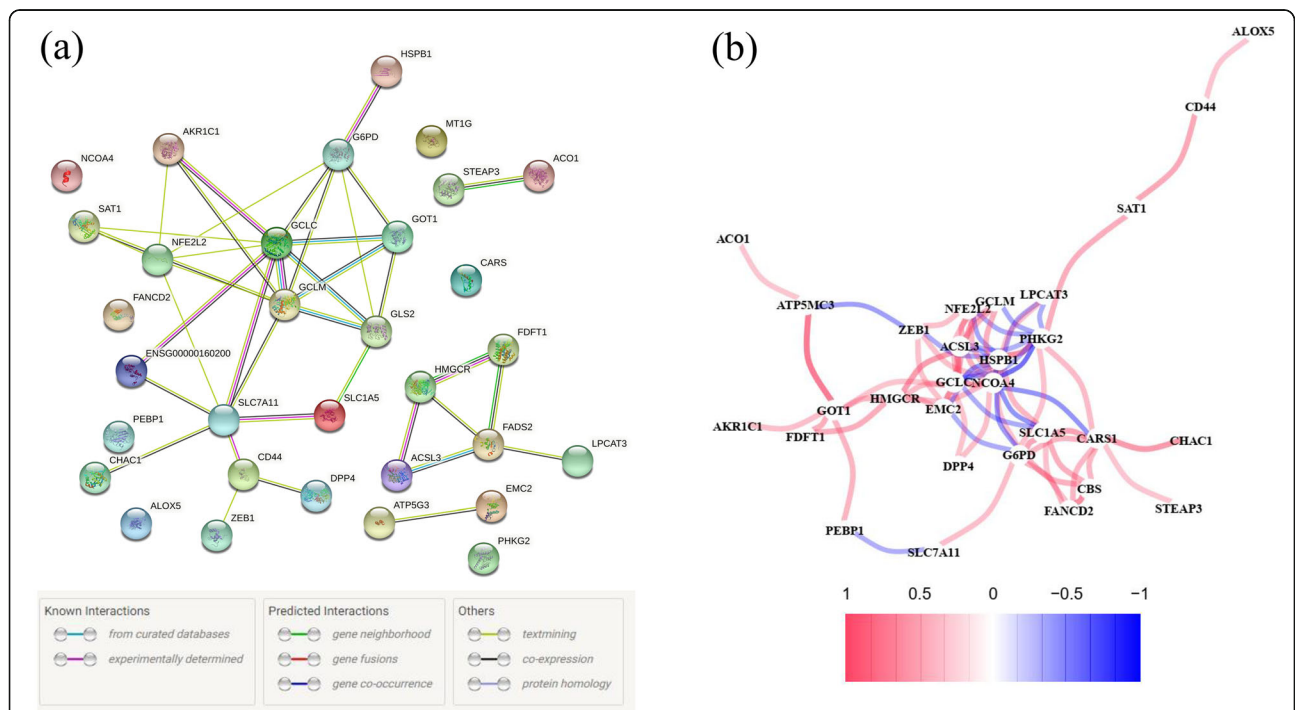


Fig. 3 Interaction networks of the prognostic ferroptosis-related DEGs in the KIRC cohort. **(A)** The PPI network downloaded from the STRING database indicated the interactions among candidate genes. **(B)** The correlation network of candidate genes, in which the correlation coefficients are represented by different colours

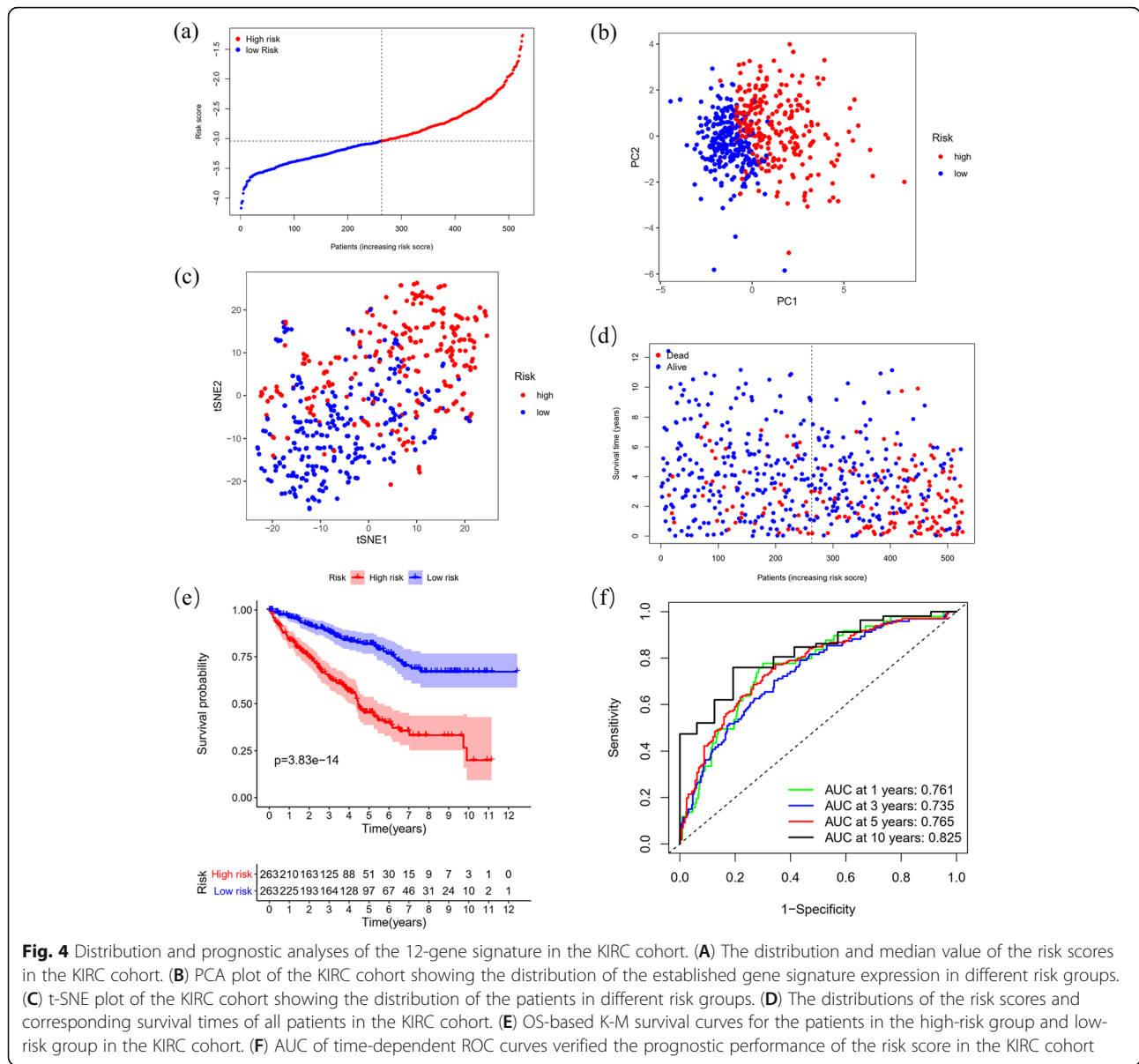


Fig. 4 Distribution and prognostic analyses of the 12-gene signature in the KIRC cohort. **(A)** The distribution and median value of the risk scores in the KIRC cohort. **(B)** PCA plot of the KIRC cohort showing the distribution of the established gene signature expression in different risk groups. **(C)** t-SNE plot of the KIRC cohort showing the distribution of the patients in different risk groups. **(D)** The distributions of the risk scores and corresponding survival times of all patients in the KIRC cohort. **(E)** OS-based K-M survival curves for the patients in the high-risk group and low-risk group in the KIRC cohort. **(F)** AUC of time-dependent ROC curves verified the prognostic performance of the risk score in the KIRC cohort

time-dependent receiver operating characteristic (ROC) analysis based on OS were performed using the “survival” package [41], the “survminer” package [42] and the “time-ROC” package [43] in R to estimate the prognostic accuracy of the gene signature in the derivation set and verify it in the validation set.

Prognostic independence of the gene signature from traditional clinical characteristics

To further assess the independent prognostic value of the established gene signature, we used univariate and multivariate Cox regression analyses to determine whether it was affected by other clinical characteristics. Several available clinical characteristics, including age, gender and TNM stage, were transformed into dichotomous variables

and included for the calculation of hazard ratios (HRs) and 95% confidence intervals (CIs) based on OS. $P < 0.05$ was considered statistically significant.

GO, KEGG and immune infiltration enrichment analyses for risk-related DEGs

According to the risk grouping, normalized gene expression matrixes of the derivation set and the validation set generated above were applied with the “limma” R package [44] to identify risk-related DEGs with the cut-off criteria of $|FC| \geq 1.5$ and $FDR < 0.05$, respectively. Risk-related DEGs were analysed with GO [45] and KEGG [46] using the “clusterProfiler” R package [47]. The top 30 enriched terms in 3 categories of GO (including biological process (BP), cellular component (CC) and

molecular function (MF)) and KEGG with the cut-off criteria of gene count > 10 and *P*-value < 0.05 in both 2 sets were intersected to obtain the overlapping enriched terms. Then, single-sample gene set enrichment analysis (ssGSEA) [48] for immune infiltration was applied with the “GSVA” R package [49] to assess the infiltration score of 16 immune cells and the activity of 13 immune-related functions. With the annotated gene sets provided in Supplementary Table S2, we quantified the immune infiltration enrichment scores for different immune cells and immune-related functions to further investigate the correlation between the risk score and immune status.

Results

Identification of prognostic ferroptosis-related DEGs in the KIRC cohort

Among 60 ferroptosis-related genes, 55 (91.67%) were differentially expressed between ccRCC samples and normal kidney samples (Fig. 2A), and 34 (56.67%) were considered OS-related in the univariate Cox regression analysis (Fig. 2B), from which 32 overlapping genes correlated to ferroptosis and OS were selected by the intersection analysis (Fig. 2C). Interactions of 32 prognostic ferroptosis-related DEGs were further visualized with the PPI and correlation networks (Fig. 3A-B).

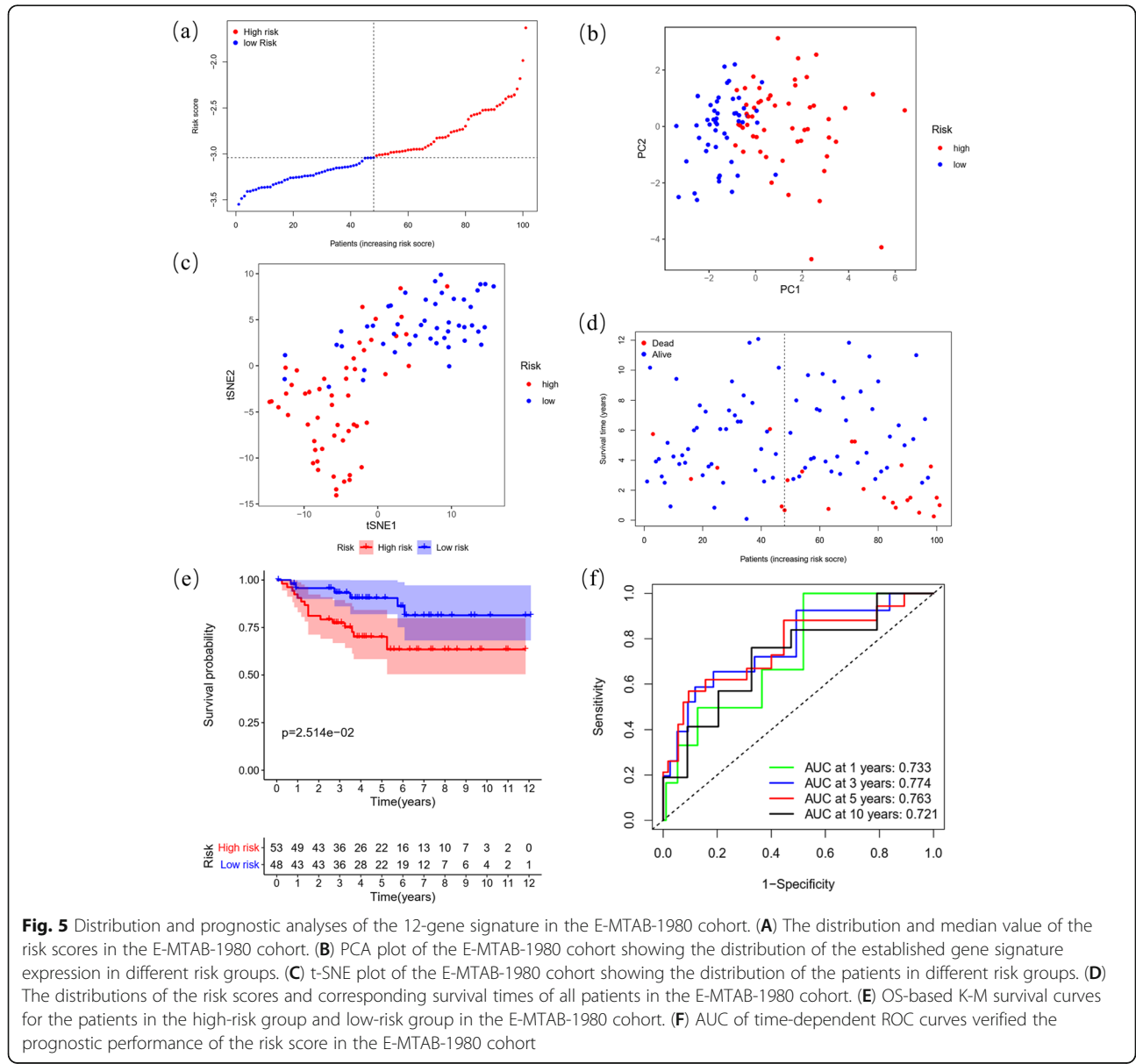


Fig. 5 Distribution and prognostic analyses of the 12-gene signature in the E-MTAB-1980 cohort. **(A)** The distribution and median value of the risk scores in the E-MTAB-1980 cohort. **(B)** PCA plot of the E-MTAB-1980 cohort showing the distribution of the established gene signature expression in different risk groups. **(C)** t-SNE plot of the E-MTAB-1980 cohort showing the distribution of the patients in different risk groups. **(D)** The distributions of the risk scores and corresponding survival times of all patients in the E-MTAB-1980 cohort. **(E)** OS-based K-M survival curves for the patients in the high-risk group and low-risk group in the E-MTAB-1980 cohort. **(F)** AUC of time-dependent ROC curves verified the prognostic performance of the risk score in the E-MTAB-1980 cohort

Establishment of a ferroptosis-related 12-gene signature in the KIRC cohort

The 32 prognostic ferroptosis-related DEGs were subjected to Lasso Cox regression analysis based on OS, and a 12-gene signature with CARS1, HMGCR, CHAC1, GOT1, CD44, STEAP3, AKR1C1, CBS, DPP4, FANCD2, SLC1A5 and NCOA4 was identified in the KIRC cohort. According to the median risk score, patients were divided into a high-risk group ($n = 263$) and a low-risk group ($n = 263$) (Fig. 4A), which were distributed into two sets in PCA and t-SNE (Fig. 4B-C). In addition, considering survival outcomes, we observed that the high-risk group had more deaths than the low-risk group (Fig. 4D). To further evaluate the prognostic value and predictive performance of the gene signature, we performed K-M survival and time-dependent ROC analyses, and both produced significant results. The K-M survival curve showed significantly worse survival outcomes for patients in the high-risk group than for patients in the low-risk group ($P = 3.83e-14$) (Fig. 4E), and the area under the curve (AUC) reached 0.761 at 1 year, 0.735 at 3 years, 0.765 at 5 years, and 0.825 at 10 years in the ROC analysis (Fig. 4F).

Validation of the prognostic predictive performance for the 12-gene signature in the E-MTAB-1980 cohort

By applying the KIRC median risk score in the E-MTAB-1980 cohort, we categorized 101 patients as either high-risk ($n = 53$) or low-risk ($n = 48$) with different PCA, t-SNE and death probability distributions similar to the KIRC cohort (Fig. 5A-D). Consistently, a positive risk-related K-M survival curve with a significant P -value ($2.514e-2$) and ROC curves with considerable AUCs (0.733 at 1 year, 0.774 at 3 years, 0.763 at 5 years, and 0.721 at 10 years) were also established as convincing validation for the gene signature (Fig. 5E-F).

Prognostic independence of the 12-gene signature from clinical characteristics

Age, gender and TNM stage were included to test the independence of the prognostic 12-gene signature in the univariate and multivariate Cox regression. As shown in the univariate Cox regression analysis, risk score and TNM stage were proven to be strong OS-related factors in both the KIRC (risk score: HR = 3.950, 95% CI = 3.031–5.147, $P < 0.001$; TNM stage: HR = 3.961, 95% CI = 2.871–5.463, $P < 0.001$) and the E-MTAB-1980

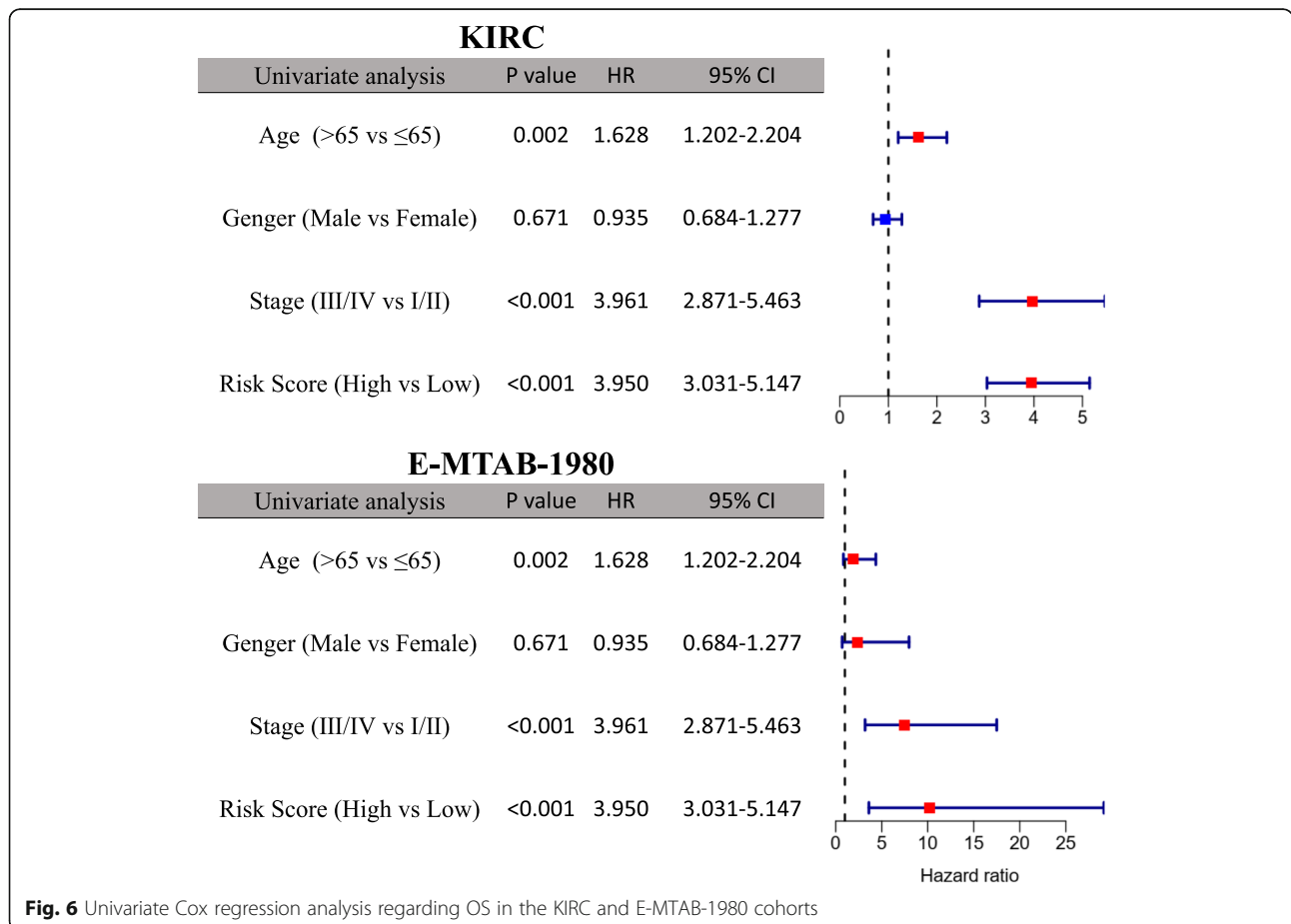


Fig. 6 Univariate Cox regression analysis regarding OS in the KIRC and E-MTAB-1980 cohorts

cohorts (risk score: HR = 10.247, 95% CI = 3.604–29.136, $P < 0.001$; TNM stage: HR = 7.472, 95% CI = 3.191–17.496, $P < 0.001$), as well as age in the KIRC cohort (HR = 1.628, 95% CI = 1.202–2.204, $P = 0.002$) (Fig. 6). After independent correction for other clinical characteristics in the multivariate Cox regression, the risk score was still a solid prognostic predictor for OS in both cohorts (KIRC: HR = 2.953, 95% CI = 2.223–3.924, $P < 0.001$; E-MTAB-1980: HR = 4.270, 95% CI = 1.465–12.439, $P = 0.008$) (Fig. 7).

GO and KEGG enrichment analyses in the KIRC and E-MTAB-1980 cohorts

After differential expression analysis between the high- and low-risk groups, 8597 DEGs significantly enriched in 958 BP, 92 CC, 155 MF and 66 KEGG terms were identified in the KIRC cohort. For the E-MTAB-1980 cohort, 1253 DEGs were significantly enriched in 605 BP, 50 CC, 76 MF and 28 KEGG terms. All significantly enriched terms are shown in Supplementary Tables S3 and S4 for the KIRC and E-MTAB-1980 cohorts, respectively. We selected the top 30 enriched terms in GO and KEGG in both cohorts and found 9, 15, 20 and 8 overlapping enriched terms in BP, CC, MF and KEGG, respectively (Figs. 8-9). As expected, several iron-related molecular functions, including metal ion transmembrane transporter activity, ion channel activity, and active ion transmembrane transporter activity,

were identified. Moreover, several immune-related terms in BP (humoral immune response), MF (cytokine receptor binding; cytokine activity) and KEGG (viral protein interaction with cytokine and cytokine receptor; IL-17 signaling pathway; cytokine-cytokine receptor interaction) were significantly enriched in both cohorts (Figs. 8-9).

Immune infiltration ssGSEA in the KIRC and E-MTAB-1980 cohorts

In the KIRC cohort, we found that 9 out of 16 immune cells had significantly higher infiltration enrichment scores in the high-risk group: CD8+ T cells, macrophages, plasmacytoid dendritic cells (pDCs), T helper cells, follicular helper T cell (Tfh), helper T cells 1 (Th1 cells), helper T cells 2 (Th2 cells), tumour infiltrating lymphocyte (TIL) and regulatory T cell (Treg), while immature dendritic cells (iDCs) and mast cells showed the opposite pattern (Fig. 10A). Similarly, the high-risk group was predicted to be significantly correlated with most immune-related functions, except for the Type II immune interferon (IFN) Response (Fig. 10B). Regarding ssGSEA in the E-MTAB-1980 cohort, we validated the significantly different infiltration scores of 3 immune cells (macrophages, mast cells and Tregs) and 1 immune-related function (antigen processing cell (APC) co-stimulation) (Fig. 10C-D).

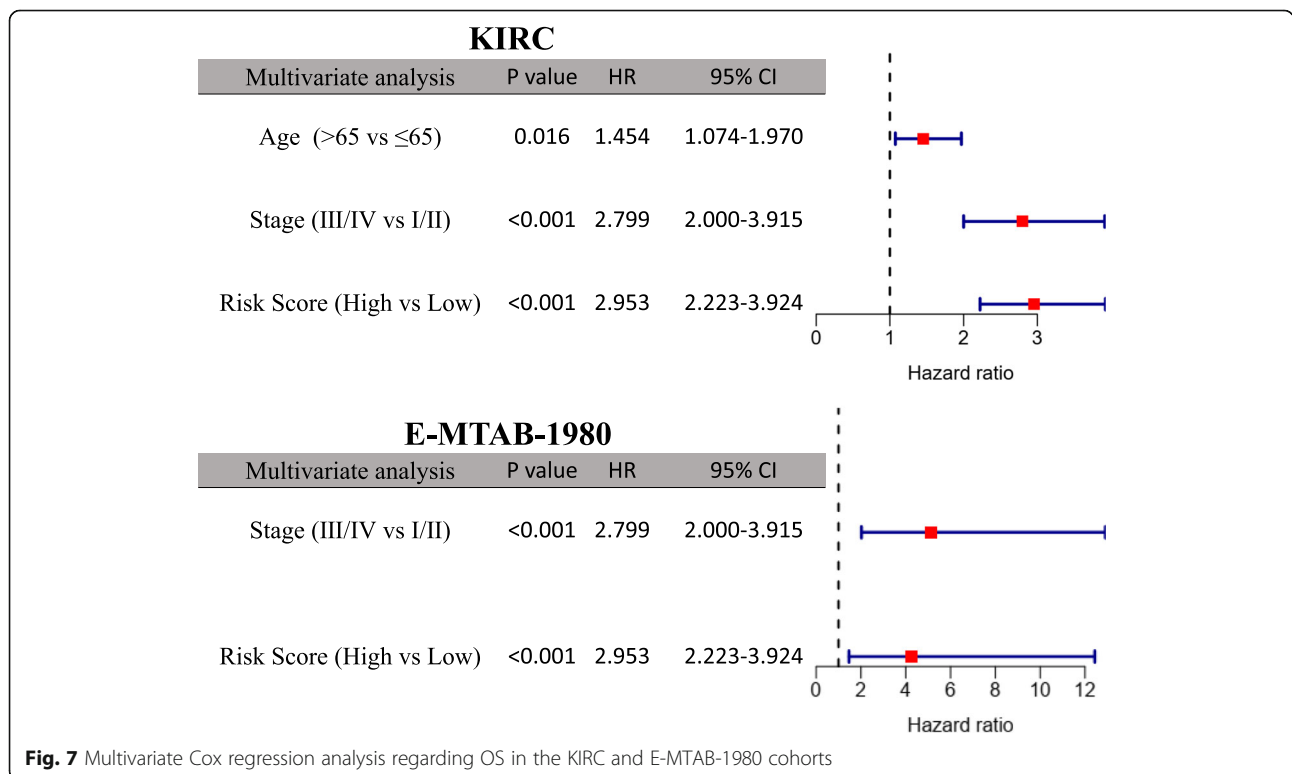
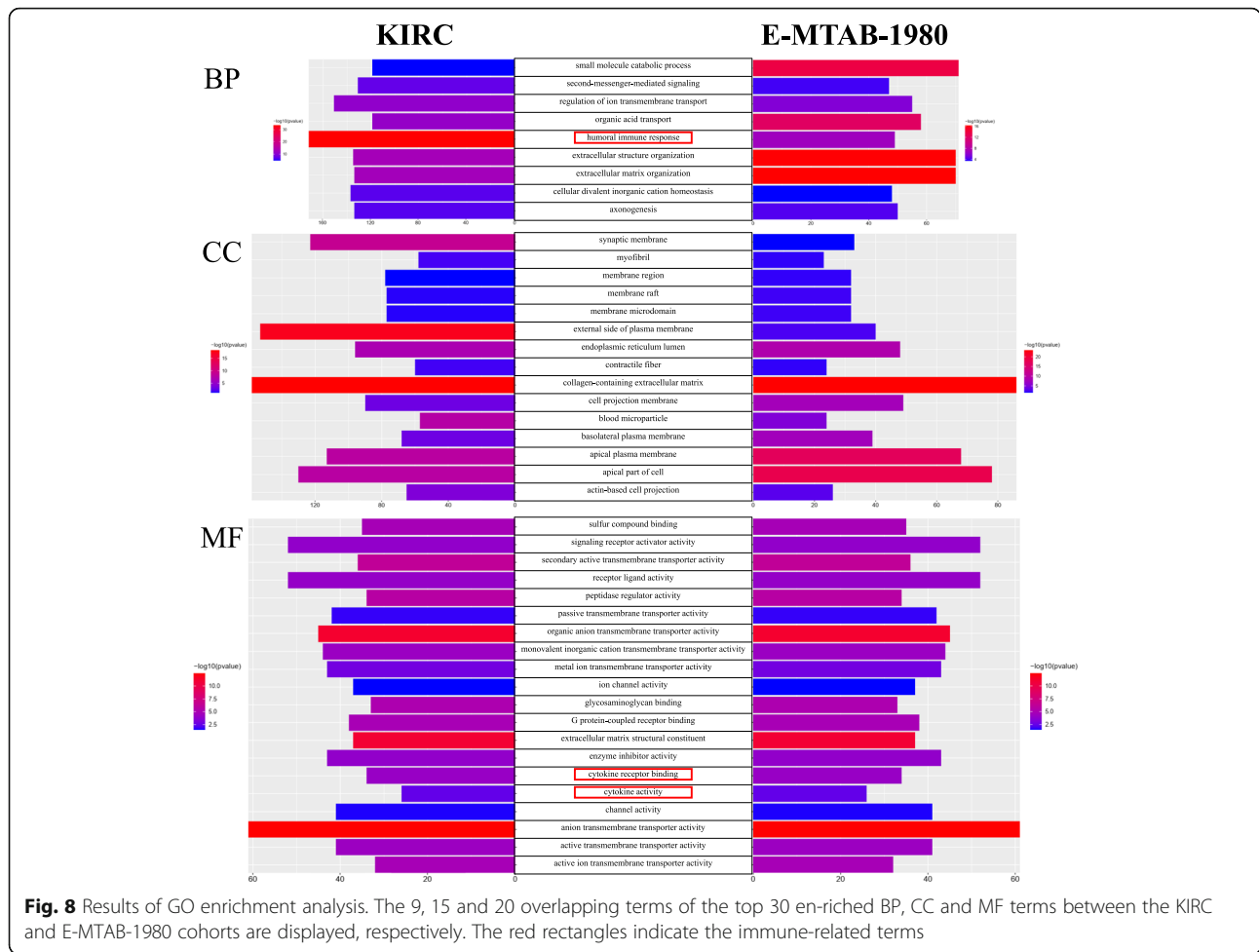


Fig. 7 Multivariate Cox regression analysis regarding OS in the KIRC and E-MTAB-1980 cohorts



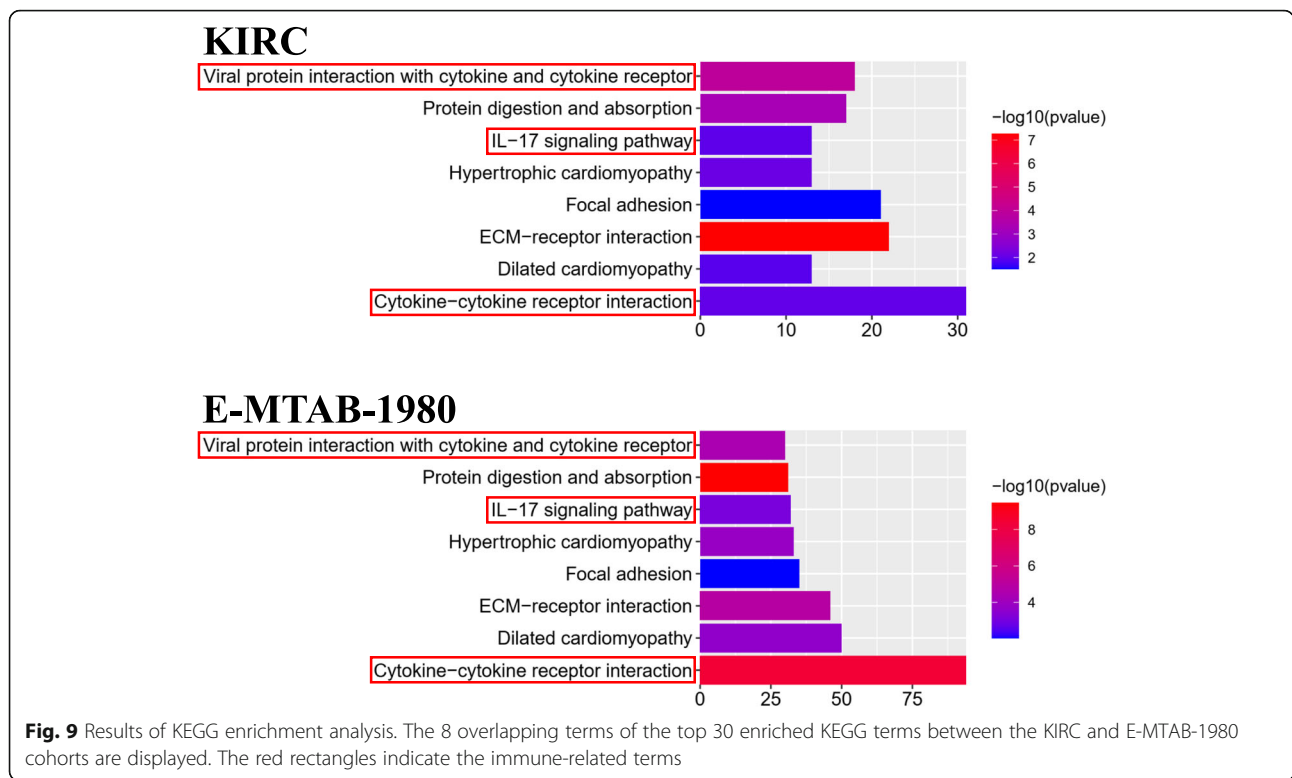
Discussion

In the current study, the expression and clinical data were retrieved from the KIRC cohort in TCGA and the E-MTAB-1980 cohort in ArrayExpress. Within 60 ferroptosis-related genes, we performed differential expression analysis and univariate Cox analysis to screen 32 prognostic DEGs, from which Lasso-penalized Cox regression analysis was applied to construct a prognostic 12-gene signature with CARS1, HMGCR, CHAC1, GOT1, CD44, STEAP3, AKR1C1, CBS, DPP4, FANCD2, SLC1A5 and NCOA4. The signature-correlated risk score of each patient in both cohorts was calculated, according to which patients were assigned to either the high- or low-risk group divided by the median risk score of the KIRC cohort. Then, the independent prognostic value of the signature was further assessed by K-M survival, ROC and Cox regression analyses in the KIRC cohort and validated in the E-MTAB-1980 cohort. Finally, risk-related DEGs were identified in both cohorts and subjected to enrichment analyses for GO, KEGG and immune infiltration. As expected, several iron-related GO and KEGG terms were significantly enriched. However, interestingly, some

immune-related terms were identified. Further immune infiltration analysis showed that 3 immune cells and 1 immune-related function were enriched in both cohorts, which supported the potential relationship between tumour immunity and ferroptosis in ccRCC.

The prognostic 12-ferroptosis-related-gene signature contains 5 protective genes (HMGCR, GOT1, AKR1C1, DPP4 and NCOA4) and 7 risk genes (CARS1, CHAC1, CD44, STEAP3, CBS, FANCD2 and SLC1A5), which can be classified as iron metabolism-related (NCOA4, STEAP3 and FANCD2), lipid metabolism-related (HMGCR, AKR1C1 and DPP4), (anti) oxidant metabolism-related (CHAC1, CD44, CBS and CARS1) and energy metabolism-related genes (GOT1 and SLC1A5) according to the potential gene-regulating function for ferroptosis [30].

In iron metabolism, NCOA4 can help elevate the levels of free iron by recruiting iron-storage protein ferritin (FTH) including ferritin light chain (FTL) and ferritin heavy chain 1 (FTH1) for lysosomal degradation and then releasing iron. As a participant in free radical formation and lipid peroxidation propagation, the accumulation of iron can increase the ferroptotic

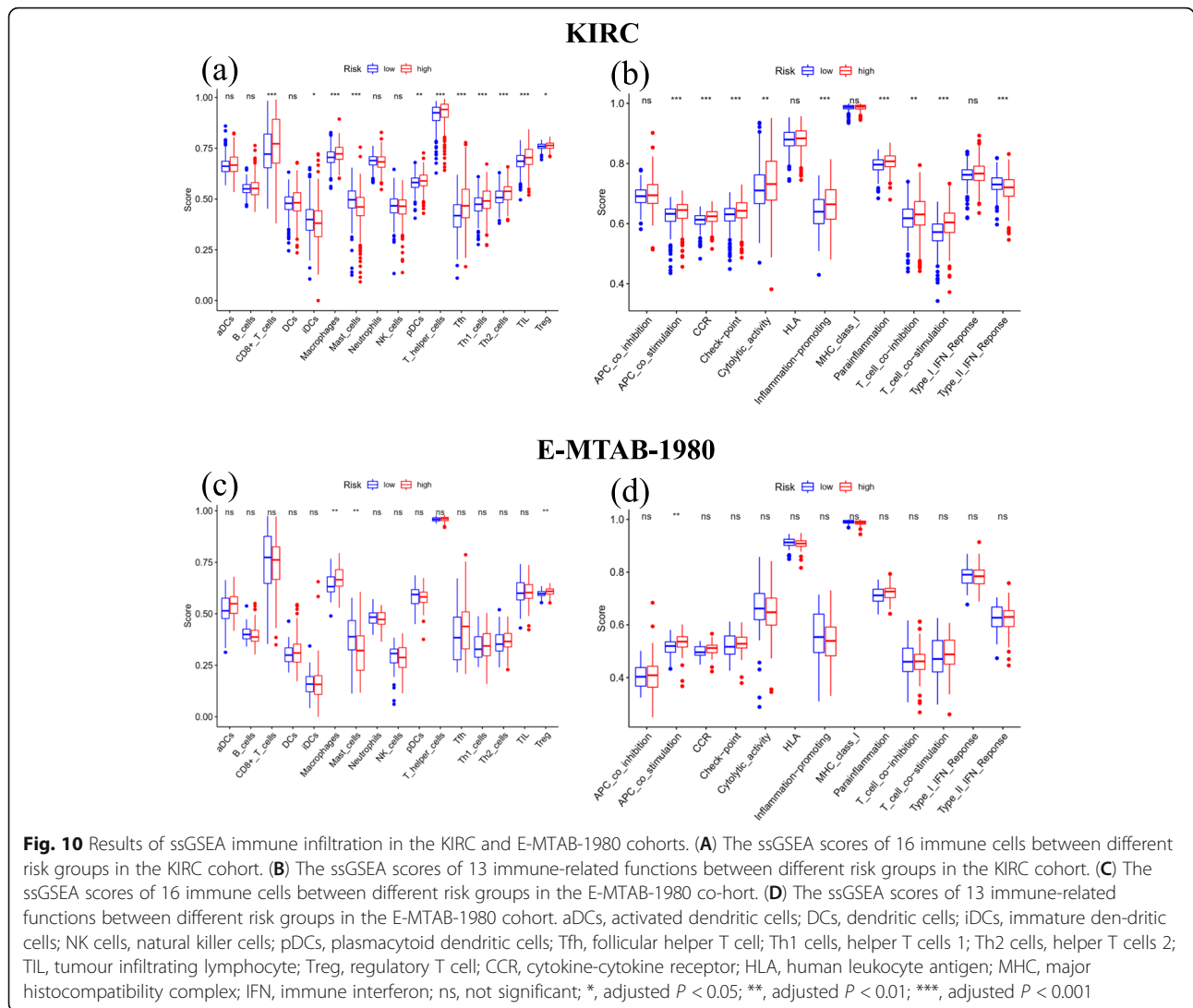


sensitivity of cells. Therefore, inhibition of NCOA4 can suppress ferroptosis induced by amino acid/cystine deprivation or erastin [50, 51]. In addition, the expression STEAP3, a metalloredutase reducing Fe³⁺ to Fe²⁺, can also be upregulated in ferroptosis. In the endosome, Fe²⁺ reduced by STEAP3 will be released into the cytosol to increase free iron and therefore participate in ferroptosis. In contrast to what was mentioned above, FANCD2 is a nuclear protein involved in DNA damage repair with a potential ability to decrease iron levels. In bone marrow stromal cells, the knockout of FANCD2 increased the expression of STEAP3 and enhanced erastin-induced ferroptosis [52].

HMGCR is a reductase that can catalyze 3-hydroxy-3-methyl-glutaryl coenzyme A (HMG-CoA) to synthesize mevalonic acid and then participate in the synthesis of sterol coenzyme Q10 (CoQ10), an endogenous suppressor of ferroptosis. A study showed that the drug inhibition of HMGCR is responsible for the enhancement of FIN56-induced ferroptosis [53]. AKR1C1 is a member of aldosterone reductase family 1 (AKR1), an aldehyde detoxification enzyme family that is involved in steroid metabolism. The overexpression of AKR1C (including AKR1C1, AKR1C2 and AKR1C3) has been proven to have an anti-ferroptotic effect through the reduction reaction converting the end products of lipid peroxides to

the corresponding nontoxic lipid-derived alcohols [54]. DPP4 is a binding protein to NOX, a participant in a membrane-bound enzyme complex that produces downstream ROS. The combination of NOX-DPP4/CD26 can cause plasma membrane lipid peroxidation and therefore result in ferroptosis, which can be blocked by p53 through DPP4 silencing in colorectal cancer cells [55]. In addition, the involvement of DPP4 and p53 was observed in Golgi stress-induced ferroptosis [56].

During (anti) oxidant metabolism in ferroptosis, cysteine serves as an initiator by providing materials for the biosynthesis of glutathione (GSH), which contributes an anti-ferroptotic effect. Extracellular cysteine can be transported into the cytosol by exchange with intracellular glutamate through the cysteine-glutamate exchange system Xc-. CHAC1 and CD44 have been suggested to interact with system Xc- and provide a pro-ferroptotic effect in Burkitt's lymphoma [57] and an anti-ferroptosis effect in human gastrointestinal cancer [17], respectively. In another way, homocysteine has an alternative transsulfuration pathway that produces cystathionine promoted by CBS and then cysteine promoted by cystathionine (CTH). In the cytoplasm, cysteine can be charged with tRNACys, which are catalysed by CARS1 and therefore result in a decrease in cysteine. A study showed that the knockdown of CARS1 can increase the compensatory transsulfuration pathway to increase cysteine and suppress ferroptosis induced by



erastin, which can be resensitized by silencing CBS [58]. Additionally, the ferroptosis-enhancing effect of suppressing CBS has been demonstrated in hepatocellular carcinoma cells [59].

GOT1 and SLC1A5 are both involved in the energy-metabolic network for ROS production in ferroptosis. In cystine deprivation- or erastin-induced ferroptosis, SLC1A5-mediated L-glutamine uptake is a critical process for the production of glutamate, which is further converted into α -ketoglutarate (α KG) by transaminase GOT1-mediated transamination [60]. The accumulation of α KG can be converted into acetyl coenzyme A (acetyl-CoA) in the cytoplasm for lipid biosynthesis and fatty acid synthesis or increase mitochondrial ROS and iron levels to promote ferroptosis [61, 62]. Immune cells are attracted and accumulated by a set of signals to help program cell death during apoptosis [63]. It is conceivable that similar signal patterns will attract APCs and

other immune cells to assist the accomplishment of ferroptosis, although solid proof is still lacking. However, an in vitro study on macrophage clearance of ferroptotic cells supported this possibility [64]. Bioinformatically, several studies have demonstrated the potential connection between RCC and immune infiltration [65, 66]. Clinically, in addition to palliative targeted therapy, considerable promising results of monotherapy with novel immunotherapies, such as immune checkpoint inhibitors (ICIs), have been observed in some advanced RCC patients [67]. Moreover, a combinatory ICI therapy of nivolumab plus ipilimumab has been approved for the phase-3 clinical trial last year [68].

In the present study, with immune annotation analysis based on risk groups, we discovered that macrophages, mast cells, Tregs and immune-related function APC costimulation were significantly enriched in both cohorts, which indicates a potential underlying modulation

between tumour immunity and ferroptosis in ccRCC. Macrophages, mast cells and Tregs are all APCs that are capable of presenting processed antigens to T cells and activating the immune response by co-stimulation. Tumour-associated macrophages (TAMs) have a dual character and have either procancer or anticancer effects in the immune system [69, 70]. As in ccRCC, it has been demonstrated that an increased density of TAMs is associated with poor clinical prognosis and aggressive tumour migration [71, 72]. Similarly, Tregs show tumour-facilitating potential in ccRCC. Tregs have been proven to have an association with worse prognosis in ccRCC [73, 74]. For mast cells, the research of Şenbaobaoğlu et al. revealed that mast cell density has an independent negative correlation with OS and progression-free survival (PFS) in ccRCC [66]. Moreover, Fu et al. observed that mast cells were independently negatively correlated with cancer-specific survival (CSS) and relapse-free survival (RFS) in ccRCC [75]. In addition, *in vitro* and *in vivo* experiments have demonstrated the angiogenesis-promoting effect of mast cells in RCC [76]. Although multiple pieces of evidence have elucidated the functions of macrophages, mast cells and Tregs in ccRCC, the underlying mechanism remains poorly characterized, and this issue in the field of ferroptosis is lacking. The relationships between the immune response and ferroptosis and how they correlate with prognosis in ccRCC still require further investigation.

Several limitations were observed in the present study. As a bioinformatics analysis, the weakness of lacking experimental and clinical validation is inevitable, as well as the various possible results from using different cut-off criteria, statistical methods or analysis tools. Additionally, establishing a prognostic model by considering a single hallmark might lead to the regrettable absence of many other promising prognostic genes.

In summary, we established a novel ferroptosis-related 12-gene signature that was proven to be an independent prognostic predictor for OS in ccRCC. Through functional annotation analyses, the gene signature was shown to be tumour immunity-correlated; however, the underlying mechanism is still poorly characterized and needs further exploration.

Abbreviations

acetyl-CoA: acetyl coenzyme A; α KG: α -ketoglutarate; AKR1: aldosterone reductase family 1; APC: antigen processing cell; AUC: area under the curve; BP: biological process; CC: cellular component; ccRCC: clear cell renal cell carcinoma; CIs: confidence intervals; CoQ10: coenzyme Q10; CSS: cancer-specific survival; CTH: cystathionine; DEGs: differentially expressed genes; FC: fold change; FDR: false discovery rate; FTH: ferritin; FTH1: ferritin heavy chain 1; FTL: ferritin light chain; GO: Gene Ontology; GSH: glutathione; HMG-CoA: 3-hydroxy-3-methyl-glutaryl coenzyme A; HRs: Hazard ratios; ICIs: immune checkpoint inhibitors; iDCs: immature dendritic cells; IFN: immune interferon; KEGG: Kyoto Encyclopedia of Genes and Genomes; K-M: Kaplan-Meier; MF: molecular function; mTOR: mammalian target of rapamycin; OS: overall survival; PCA: principal component analysis;

pDCs: plasmacytoid dendritic cells; PFS: progression-free survival; PPI: protein-protein interaction; RCC: renal cell carcinoma; RCD: regulated cell death; RFS: relapse-free survival; ROC: receiver operating characteristic; ROS: reactive oxygen species; ssGSEA: single-sample gene set enrichment analysis; TAMs: Tumour-associated macrophages; TCGA: the cancer genome atlas; Tfh: follicular helper T cell; Th1 cells: helper T cells 1; Th2 cells: helper T cells 2; TIL: tumour infiltrating lymphocyte; TKIs: tyrosine kinase inhibitors; Treg: regulatory T cell; t-SNE: t-distributed stochastic neighbour embedding

Supplementary Information

The online version contains supplementary material available at <https://doi.org/10.1186/s12885-021-08559-0>.

Additional file 1.

Acknowledgments

The manuscript's preprint can be found in the link below: <https://www.researchsquare.com/article/rs-153932/v1>.

Authors' contributions

Conceptualization, Peilin Shen; Data curation, Mingen Lin, Dehua Ou and Zhuangkai Huang; Formal analysis, Yingkai Hong and Dehua Ou; Methodology, Peilin Shen; Project administration, Peilin Shen; Software, Yingkai Hong and Mingen Lin; Visualization, Yingkai Hong and Mingen Lin; Writing – original draft, Yingkai Hong; Writing – review & editing, Peilin Shen. All authors read and approved the final manuscript.

Funding

This work was supported by the Guangdong Medical Research Foundation (A2018103 and 201711795717822), Shantou Science and Technology Project (180404094011031) and Natural Science Foundation of Guangdong Province (No. 2015A030310078).

Availability of data and materials

The datasets analyzed for this study can be found in the KIRC project in TCGA database (<https://portal.gdc.cancer.gov/repository>) and E-MTAB-1980 cohort in ArrayExpress database (<https://www.ebi.ac.uk/arrayexpress/experiments/E-MTAB-1980/>). The literature survey data from this study can be request from the corresponding author Peilin Shen.

Declarations

Ethics approval and consent to participate

Not applicable.

Consent for publication

Not applicable.

Competing interests

The authors declare that the research was conducted in the absence of any commercial or financial relationships that could be construed as a potential conflict of interest.

Author details

¹Department of Urology, The First Affiliated Hospital of Shantou University Medical College, Shantou, People's Republic of China 515041. ²Shantou University Medical College, Shantou, People's Republic of China.

Received: 24 April 2021 Accepted: 18 June 2021

Published online: 19 July 2021

References

1. Wild CPWE, Stewart BW. World Cancer report: Cancer research for Cancer prevention. Lyon: International Agency for Research on Cancer; 2020.
2. Prasad SR, Humphrey PA, Catena JR, Narra VR, Strigley JR, Cortez AD, et al. Common and uncommon histologic subtypes of renal cell carcinoma: imaging Spectrum with pathologic correlation. *Radiographics*. 2006;26(6):1795–806. <https://doi.org/10.1148/rg.266065010>.

3. Rao A, Wiggins C, Lauer RC. Survival outcomes for advanced kidney cancer patients in the era of targeted therapies. *Case Rep Rheumatol*. 2018;6(9):165.
4. Gill DM, Agarwal N, Vaishampayan U. Evolving treatment paradigm in metastatic renal cell carcinoma. *Am Soc Clin Oncol Educ Book Am Soc Clin Oncol Annu Mee*. 2017;37(37):319–29. https://doi.org/10.1200/EDBK_174469.
5. Manz DH, Blanchette NL, Paul BT, Torti FM, Torti SV. Iron and cancer: recent insights. *Ann N Y Acad Sci*. 2016;1368(1):149–61.
6. Huang X. Iron overload and its association with cancer risk in humans: evidence for iron as a carcinogenic metal. *Mutat Res*. 2003;533(1–2):153–71. <https://doi.org/10.1016/j.mrfmmm.2003.08.023>.
7. Weinlich R, Oberst A, Beere HM, Green DR. Necroptosis in development, inflammation and disease. *Nat Rev Mol Cell Biol*. 2016;18(2):127.
8. Bergsbaken T, Fink SL, Cookson BT. Pyroptosis: host cell death and inflammation. *Nat Rev Microbiol*. 2009;7(2):99–109. <https://doi.org/10.1038/nrmicro2070>.
9. Song X, Zhu S, Xie Y, Liu J, Sun L, Zeng D, et al. JTC801 induces pH-dependent death specifically in Cancer cells and slows growth of tumors in mice. *Gastroenterology*. 2018;154(5):1480–93. <https://doi.org/10.1053/j.gastro.2017.12.004>.
10. Liu J, Kuang F, Kang R, Tang D. Alkaliptosis: a new weapon for cancer therapy. *Can Gene Ther*. 2020;27(5):267–9.
11. Dixon SJ, Lemberg KM, Lamprecht MR, Skouta R, Zaitsev EM, Gleason CE, et al. Ferroptosis: an iron-dependent form of nonapoptotic cell death. *Cell*. 2012;149(5):1060–72. <https://doi.org/10.1016/j.cell.2012.03.042>.
12. Chen X, Li J, Kang R, Klionsky DJ, Tang D. Ferroptosis: machinery and regulation. *Autophagy*. 2020;26:1–28.
13. Tang D, Chen X, Kang R, Kroemer G. Ferroptosis: molecular mechanisms and health implications. *Cell Res*. 2021;31(2):107–25.
14. Yang WS, Sriramaratnam R, Welsch ME, Shimada K, Skouta R, Viswanathan VS, et al. Regulation of Ferroptotic Cancer cell death by GPX4. *Cell*. 2014;156(1–2):317–31. <https://doi.org/10.1016/j.cell.2013.12.010>.
15. Vasuri F, Visani M, Acquaviva G, Brand T, Fiorentino M, Pession A, et al. Role of microRNAs in the main molecular pathways of hepatocellular carcinoma. *World J Gastroenterol*. 2018;24(25):2647–60. <https://doi.org/10.3748/wjg.v24.i25.2647>.
16. Hao S, Yu J, He W, Huang Q, Zhao Y, Liang B, et al. Cysteine Dioxygenase 1 mediates Erastin-induced Ferroptosis in human gastric Cancer cells. *Neoplasia*. 2017;19(12):1022–32. <https://doi.org/10.1016/j.neo.2017.10.005>.
17. Ishimoto T, Nagano O, Yae T, Tamada M, Motohara T, Oshima H, et al. CD44 variant regulates redox status in cancer cells by stabilizing the xCT subunit of system xc(–) and thereby promotes tumor growth. *Cancer Cell*. 2011;19(3):387–400. <https://doi.org/10.1016/j.ccr.2011.01.038>.
18. Basuli D, Tesfay L, Deng Z, Paul B, Torti SV. Iron addiction: A novel therapeutic target in ovarian cancer. *Oncogene*. 2017;36(29):4089–99.
19. Greenshields AL, Shepherd TG, Hoskin DW. Contribution of reactive oxygen species to ovarian cancer cell growth arrest and killing by the anti-malarial drug artesunate. *Mol Cancer*. 2017;56(1):75–93.
20. Ma S, Dielschneider RF, Henson ES, Xiao W, Gibson SB. Ferroptosis and autophagy induced cell death occur independently after siramesine and lapatinib treatment in breast cancer cells. *PLoS One*. 2017;12(8):e0182921. <https://doi.org/10.1371/journal.pone.0182921>.
21. Zhu HY, Huang ZX, Chen GQ, Sheng F, Zheng YS. Typhaneoside prevents acute myeloid leukemia (AML) through suppressing proliferation and inducing ferroptosis associated with autophagy. *Biochem Biophys Res Commun*. 2019;516(4):1265–71. <https://doi.org/10.1016/j.bbrc.2019.06.070>.
22. Xie Y, Hou W, Song X, Yu Y, Huang J, Sun X, et al. Ferroptosis: process and function. *Cell Death & Differentiation*. 2016;23(3):369–79. <https://doi.org/10.1038/cdd.2015.158>.
23. Haase VH. Hypoxic regulation of erythropoiesis and iron metabolism. *American journal of physiology Renal physiology*. 2010;299(1):F1–13. <https://doi.org/10.1152/ajprenal.00174.2010>.
24. Zhang S, Chang W, Wu H, Wang YH, Wang ZP. Pan-cancer analysis of iron metabolic landscape across the Cancer genome atlas. *J Cell Physiol*. 2020;235(2):1013–24.
25. Moon D, Kim J, Yoon SP. Yeast extract inhibits the proliferation of renal cell carcinoma cells via regulation of iron metabolism. *Mol Med Rep*. 2019;20(4):3933–41. <https://doi.org/10.3892/mmr.2019.10593>.
26. Team RC. R: A language and environment for statistical computing. R Foundation for Statistical Computing, Vienna. 2020 [Available from: <https://www.R-project.org/>].
27. Stockwell BR, Friedmann Angeli JP, Bayir H, Bush AI, Conrad M, Dixon SJ, et al. Ferroptosis: a regulated cell death Nexus linking metabolism, redox biology, and disease. *Cell*. 2017;171(2):273–85. <https://doi.org/10.1016/j.cell.2017.09.021>.
28. Bersuker K, Hendricks JM, Li Z, Magtanong L, Ford B, Tang PH, et al. The CoQ oxidoreductase FSP1 acts parallel to GPX4 to inhibit ferroptosis. *Nature*. 2019;575(7784):688–92. <https://doi.org/10.1038/s41586-019-1705-2>.
29. Doll S, Freitas FP, Shah R, Aldrovandi M, da Silva MC, Ingold I, et al. FSP1 is a glutathione-independent ferroptosis suppressor. *Nature*. 2019;575(7784):693–8. <https://doi.org/10.1038/s41586-019-1707-0>.
30. Hassannia B, Vandenabeele P, Vanden BT. Targeting Ferroptosis to Iron out Cancer. *Cancer Cell*. 2019;35(6):830–49. <https://doi.org/10.1016/j.ccell.2019.04.002>.
31. Robinson MD, McCarthy DJ, Smyth GK. edgeR: a Bioconductor package for differential expression analysis of digital gene expression data. *Bioinformatics (Oxford, England)*. 2010;26(11):139–40.
32. Kolde R. pheatmap: Pretty Heatmaps. R package version 1.0.12. 2019 [Available from: <https://CRAN.R-project.org/package=pheatmap>].
33. Dusa A. venn: Draw Venn Diagrams. R package version 1.9. 2020 [Available from: <https://CRAN.R-project.org/package=venn>].
34. Szklarczyk D, Gable AL, Lyon D, Junge A, Wyder S, Huerta-Cepas J, et al. STRING v11: protein-protein association networks with increased coverage, supporting functional discovery in genome-wide experimental datasets. *Nucleic Acids Res*. 2019;47(D1):D607–d13. <https://doi.org/10.1093/nar/gky1131>.
35. Csardi G, Nepusz T. The Igraph Software Package for Complex Network Research. *Inter J Complex Syst*. 2005;1695(5):1–9.
36. Wickham H. Reshaping data with the reshape package. *J Stat Softw*. 2007;21:1–20.
37. Simon N, Friedman J, Hastie T, Tibshirani R. Regularization paths for Cox's proportional hazards model via coordinate descent. *J Stat Softw*. 2011;39(5):1–13. <https://doi.org/10.18637/jss.v039.i05>.
38. Tibshirani R. The lasso method for variable selection in the cox model. *Stat Med*. 1997;16(4):385–95. [https://doi.org/10.1002/\(SICI\)1097-0258\(19970228\)16:4<385::AID-SIM380>3.0.CO;2-3](https://doi.org/10.1002/(SICI)1097-0258(19970228)16:4<385::AID-SIM380>3.0.CO;2-3).
39. Friedman J, Hastie T, Tibshirani R. Regularization paths for generalized linear models via coordinate descent. *J Stat Softw*. 2010;33(1):1–22.
40. Krijthe JH. Rtsne: T-Distributed Stochastic Neighbor Embedding using a Barnes-Hut Implementation 2015 [Available from: <https://github.com/jkrijthe/Rtsne>].
41. T T. A Package for Survival Analysis in R. R package version 3.2–7 2020 [Available from: <https://CRAN.R-project.org/package=survival>].
42. Kassambara A, Kosinski M, Biecek P. survminer: Drawing Survival Curves using 'ggplot2'. R package version 0.4.8 2020 [Available from: <https://CRAN.R-project.org/package=survminer>].
43. Blanche P, Dartigues JF, Jacqmin-Gadda H. Estimating and comparing time-dependent areas under receiver operating characteristic curves for censored event times with competing risks. *Stat Med*. 2013;32(30):5381–97. <https://doi.org/10.1002/sim.5958>.
44. Ritchie ME, Phipson B, Wu D, Hu Y, Law CW, Shi W, et al. limma powers differential expression analyses for RNA-sequencing and microarray studies. *Nucleic Acids Res*. 2015;43(7):e47.
45. Gene OC, Mul De R N. The Gene Ontology (GO) project in 2006. *Nucleic Acids Res*. 2006;1;34(Database issue):D322–6.
46. Ogata H, Goto S, Sato K, Fujibuchi W, Bono H, Kanehisa M. KEGG: Kyoto encyclopedia of genes and genomes. *Nucleic Acids Res*. 1999;27(1):29–34. <https://doi.org/10.1093/nar/27.1.29>.
47. Yu G, Wang LG, Han Y, He QY. clusterProfiler: an R package for comparing biological themes among gene clusters. *Omics : a journal of integrative biology*. 2012;16(5):284–7. <https://doi.org/10.1089/omi.2011.0118>.
48. Rooney MS, Shukla SA, Wu CJ, Getz G, Hacohen N. Molecular and genetic properties of tumors associated with local immune cytolytic activity. *Cell*. 2015;160(1–2):48–61. <https://doi.org/10.1016/j.cell.2014.12.033>.
49. Hänzelmann S, Castelo R, Guinney J. GSEA: gene set variation analysis for microarray and RNA-seq data. *BMC bioinformatics*. 2013;14(1):7. <https://doi.org/10.1186/1471-2105-14-7>.
50. Gao M, Monian P, Pan Q, Zhang W, Xiang J, Jiang X. Ferroptosis is an autophagic cell death process. *Cell Res*. 2016;26(9):1021–32. <https://doi.org/10.1038/cr.2016.95>.
51. Hou W, Xie Y, Song X, Sun X, Lotze MT, Zeh HJ 3rd, et al. Autophagy promotes ferroptosis by degradation of ferritin. *Autophagy*. 2016;12(8):1425–8. <https://doi.org/10.1080/15548627.2016.1187366>.

52. Song X, Xie Y, Kang R, Hou W, Sun X, Epperly MW, et al. FANCD2 protects against bone marrow injury from ferroptosis. *Biochem Biophys Res Commun*. 2016;480(3):443–9. <https://doi.org/10.1016/j.bbrc.2016.10.068>.
53. Shimada K, Skouta R, Kaplan A, Yang WS, Hayano M, Dixon SJ, et al. Global survey of cell death mechanisms reveals metabolic regulation of ferroptosis. *Nat Chem Biol*. 2016;12(7):497–503. <https://doi.org/10.1038/nchembio.2079>.
54. Dixon SJ, Patel DN, Welsch M, Skouta R, Lee ED, Hayano M, et al. Pharmacological inhibition of cystine-glutamate exchange induces endoplasmic reticulum stress and ferroptosis. *eLife*. 2014;3:e02523. <https://doi.org/10.7554/eLife.02523>.
55. Xie Y, Zhu S, Song X, Sun X, Fan Y, Liu J, et al. The tumor suppressor p53 limits Ferroptosis by blocking DPP4 activity. *Cell Rep*. 2017;20(7):1692–704. <https://doi.org/10.1016/j.celrep.2017.07.055>.
56. Alborzinia H, Ignashkova TI, Dejure FR, Gendarme M, Theobald J, Wöflf S, et al. Golgi stress mediates redox imbalance and ferroptosis in human cells. *Communications biology*. 2018;1(1):210. <https://doi.org/10.1038/s42003-018-0212-6>.
57. Wang N, Zeng GZ, Yin JL, Bian ZX. Artesunate activates the ATF4-CHOP-CHAC1 pathway and affects ferroptosis in Burkitt's lymphoma. *Biochem Biophys Res Commun*. 2019;519(3):533–9. <https://doi.org/10.1016/j.bbrc.2019.09.023>.
58. Hayano M, Yang WS, Corn CK, Pagano NC, Stockwell BR. Loss of cysteinyl-tRNA synthetase (CARS) induces the transsulfuration pathway and inhibits ferroptosis induced by cystine deprivation. *Cell Death Differ*. 2016;23(2):270–8. <https://doi.org/10.1038/cdd.2015.93>.
59. Wang L, Cai H, Hu Y, Liu F, Huang S, Zhou Y, et al. A pharmacological probe identifies cystathionine β -synthase as a new negative regulator for ferroptosis. *Cell Death Dis*. 2018;9(10):1005. <https://doi.org/10.1038/s41419-018-1063-2>.
60. Gao M, Monian P, Quadri N, Ramasamy R, Jiang X. Glutaminolysis and transferrin regulate Ferroptosis. *Mol Cell*. 2015;59(2):298–308. <https://doi.org/10.1016/j.molcel.2015.06.011>.
61. Lee H, Zandkarimi F, Zhang Y, Meena JK, Kim J, Zhuang L, et al. Energy-stress-mediated AMPK activation inhibits ferroptosis. *Nat Cell Biol*. 2020;22(2):225–34. <https://doi.org/10.1038/s41556-020-0461-8>.
62. Shin D, Lee J, You JH, Kim D, Roh JL. Dihydroliipoamide dehydrogenase regulates cystine deprivation-induced ferroptosis in head and neck cancer. *Redox Biol*. 2020;30:101418. <https://doi.org/10.1016/j.redox.2019.101418>.
63. Elliott MR, Ravichandran KS. The dynamics of apoptotic cell clearance. *Dev Cell*. 2016;38(2):147–60. <https://doi.org/10.1016/j.devcel.2016.06.029>.
64. Klöditz K, Fadeel B. Three cell deaths and a funeral: macrophage clearance of cells undergoing distinct modes of cell death. *Cell death discovery*. 2019;5(1):65. <https://doi.org/10.1038/s41420-019-0146-x>.
65. Zhang S, Zhang E, Long J, Hu Z, Peng J, Liu L, et al. Immune infiltration in renal cell carcinoma. *Cancer Sci*. 2019;110(5):1564–72. <https://doi.org/10.1111/cas.13996>.
66. Şenbabaoğlu Y, Gejman RS, Winer AG, Liu M, Van Allen EM, de Velasco G, et al. Tumor immune microenvironment characterization in clear cell renal cell carcinoma identifies prognostic and immunotherapeutically relevant messenger RNA signatures. *Genome Biol*. 2016;17(1):231. <https://doi.org/10.1186/s13059-016-1092-z>.
67. Joseph RW, Chatta G, Vaishampayan U. Nivolumab treatment for advanced renal cell carcinoma: considerations for clinical practice. *Urol Oncol*. 2017;35(4):142–8. <https://doi.org/10.1016/j.urolonc.2017.01.017>.
68. Cella D, Grünwald V, Escudier B, Hammers HJ, George S, Nathan P, et al. Patient-reported outcomes of patients with advanced renal cell carcinoma treated with nivolumab plus ipilimumab versus sunitinib (CheckMate 214): a randomised, phase 3 trial. *The Lancet Oncology*. 2019;20(2):297–310. [https://doi.org/10.1016/S1470-2045\(18\)30778-2](https://doi.org/10.1016/S1470-2045(18)30778-2).
69. Kitamura T, Qian BZ, Pollard JW. Immune cell promotion of metastasis. *Nat Rev Immunol*. 2015;15(2):73–86. <https://doi.org/10.1038/nri3789>.
70. Sica A, Larghi P, Mancino A, Rubino L, Porta C, Totaro MG, et al. Macrophage polarization in tumour progression. *Semin Cancer Biol*. 2008;18(5):349–55. <https://doi.org/10.1016/j.semcancer.2008.03.004>.
71. Komohara Y, Hasita H, Ohnishi K, Fujiwara Y, Suzu S, Eto M, et al. Macrophage infiltration and its prognostic relevance in clear cell renal cell carcinoma. *Cancer Sci*. 2011;102(7):1424–31. <https://doi.org/10.1111/j.1349-7006.2011.01945.x>.
72. Kadamoto S, Izumi K, Hiratsuka K, Nakano T, Naito R, Makino T, et al. Tumor-Associated Macrophages Induce Migration of Renal Cell Carcinoma Cells via Activation of the CCL20-CCR6 Axis. *Cancers*. 2019;30;12(1):89.
73. Nakayama T, Saito K, Kumagai J, Nakajima Y, Kijima T, Yoshida S, et al. Higher serum C-reactive protein level represents the immunosuppressive tumor microenvironment in patients with clear cell renal cell carcinoma. *Clin Genitourin cancer*. 2018;16(6):e1151–e8. <https://doi.org/10.1016/j.clgc.2018.07.027>.
74. Li JF, Chu YW, Wang GM, Zhu TY, Rong RM, Hou J, et al. The prognostic value of peritumoral regulatory T cells and its correlation with intratumoral cyclooxygenase-2 expression in clear cell renal cell carcinoma. *BJU Int*. 2009;103(3):399–405. <https://doi.org/10.1111/j.1464-410X.2008.08151.x>.
75. Fu H, Zhu Y, Wang Y, Liu Z, Zhang J, Wang Z, et al. Tumor infiltrating mast cells (TIMs) confers a marked survival advantage in nonmetastatic clear-cell renal cell carcinoma. *Ann Surg Oncol*. 2017;24(5):1435–42. <https://doi.org/10.1245/s10434-016-5702-5>.
76. Chen Y, Li C, Xie H, Fan Y, Yang Z, Ma J, et al. Infiltrating mast cells promote renal cell carcinoma angiogenesis by modulating PI3K→AKT→GSK3 β →AM signaling. *Oncogene*. 2017;36(20):2879–88. <https://doi.org/10.1038/ncr.2016.442>.

Publisher's Note

Springer Nature remains neutral with regard to jurisdictional claims in published maps and institutional affiliations.

Ready to submit your research? Choose BMC and benefit from:

- fast, convenient online submission
- thorough peer review by experienced researchers in your field
- rapid publication on acceptance
- support for research data, including large and complex data types
- gold Open Access which fosters wider collaboration and increased citations
- maximum visibility for your research: over 100M website views per year

At BMC, research is always in progress.

Learn more biomedcentral.com/submissions

